RESEARCH ARTICLE

Benefits of collocating vertical-axis and horizontal-axis wind turbines in large wind farms

Shengbai Xie[1], Cristina L. Archer[1], Niranjan Ghaisas[2] and Charles Meneveau[3]

[1] College of Earth, Ocean, and Environment, University of Delaware, USA
[2] Center for Turbulence Research, Stanford University, USA
[3] Department of Mechanical Engineering, Johns Hopkins University, USA

ABSTRACT

In this study, we address the benefits of a vertically staggered (VS) wind farm, in which vertical-axis and horizontal-axis wind turbines are collocated in a large wind farm. The case study consists of 20 small vertical-axis turbines added around each large horizontal-axis turbine. Large-eddy simulation is used to compare power extraction and flow properties of the VS wind farm versus a traditional wind farm with only large turbines. The VS wind farm produces up to 32% more power than the traditional one, and the power extracted by the large turbines alone is increased by 10%, caused by faster wake recovery from enhanced turbulence due to the presence of the small turbines. A theoretical analysis based on a top-down model is performed and compared with the large-eddy simulation. The analysis suggests a nonlinear increase of total power extraction with increase of the loading of smaller turbines, with weak sensitivity to various parameters, such as size, and type aspect ratio, and thrust coefficient of the vertical-axis turbines. We conclude that vertical staggering can be an effective way to increase energy production in existing wind farms. Copyright © 2016 John Wiley & Sons, Ltd.

1. INTRODUCTION

With the increasing demand for renewable energy globally, wind farms, especially offshore wind farms, have continued to increase in size. It is well known that the energy loss in a large wind farm can be due in large part to the interactions between wind turbines and wind turbine wakes.[1–6] Wake losses can be reduced by using a staggered layout of the wind turbines in the horizontal directions. A wind farm is called 'horizontally staggered' when wind turbines in consecutive rows are not aligned behind each other along the wind direction. Wind direction effects have been systematically studied for the Horns Rev offshore wind farm by Porté-Agel *et al.*[7] using large-eddy simulation (LES). They found that even small changes in wind direction can have strong impacts on the total wind farm's power output. Chamorro *et al.*[8] used wind tunnel measurements of miniature turbine models to study turbulent properties of a horizontally staggered wind farm. They found that turbulence in the horizontally staggered wind farm resembles that in the wake of a single turbine, which is substantially different from that in an aligned configuration. Moreover, the overall power output was improved by about 10% in the horizontally staggered farm. The variations in momentum, scalar and kinetic energy fluxes between aligned and horizontally staggered model wind farms have been revealed by the experimental study of Markfort *et al.*[9] From both LES and wind tunnel experiments of 30 miniature wind turbines, Wu and Porté-Agel[10] found that the horizontally staggered layout leads to higher local wind speed, lower turbulence intensity and consequently higher turbine efficiency. Stevens *et al.*[6] used LES to study the influence of the alignment of wind turbine rows inside a large wind farm and found an increase in power generation up to 40% by an intermediate alignment configuration. The effects of spacing and horizontal staggering of wind turbines in the Lillgrund wind farm (in Sweden) have been systematically studied using

LES by Archer *et al.*,[11] where they found that total power generation was increased by 13% in the horizontally staggered layout and that the capacity factor was improved by 33% by combining both staggering and larger spacing.

Besides the horizontal staggering, the effects of staggering wind turbines in the vertical direction have also been studied in a few previous works. Chamorro *et al.*[12] studied a model wind farm consisting of miniature horizontal-axis wind turbines (HAWTs) of two sizes (i.e., two hub heights and rotor areas). Distinctive flow features were observed, which impacted power harvesting and turbulence loading. The effects of variable hub heights (with the same rotor area) of HAWTs were investigated experimentally by Vested *et al.*,[13] and 25% higher power was reported for the variable-height wind farm than for the traditional one.

In this study, out of the many possible vertical staggering types, a new approach is proposed, hereafter referred to simply as VS, which is particularly feasible for existing wind farms, in which neither the position nor the height of the existing HAWTs can be changed. Given a control wind farm comprising of traditional, large HAWTs, all with the same hub height, the space between the large turbines is filled with much smaller, shorter and lower capacity wind turbines, e.g., vertical-axis wind turbines (VAWT). The smaller turbines are used to capture the lower, but (for the most part) undisturbed winds that blow below the rotor tips of the large turbines. The smaller turbines can have vertical or horizontal axes of rotation, but the former are studied here because of their low cost and wide availability today in the low-capacity market.[14] There has been considerable recent interest in VAWT wind farms.[15] The major issue here is whether or not the presence of the layer of smaller turbines would adversely affect the energy harvested by the large HAWTS.

In this study, the VS wind farm is studied with advanced numerical simulations and with an analytical model and its performance is evaluated against its traditional counterpart, a HAWT farm in which no vertical staggering is used.

2. NUMERICAL SIMULATIONS

2.1. Methods and setup

Large-eddy simulation is used here to study the staggering of a wind farm in the vertical. LES is a numerical technique that resolves the large-scale flow motions and includes the effects of small-scale eddies via sub-grid scale models.[16] In this study, the LES model used is a pseudo-spectral version of the wind turbine and turbulence simulator developed at University of Delaware.[17] For solving the filtered Navier–Stokes equations, the Fourier series-based spectral method is used in the horizontal directions with periodic boundary conditions, and the second-order finite difference method is used in the vertical direction. The 2/3 rule is implemented for elimination of the aliasing errors.[18] A second-order Adams–Bashforth scheme is used for time integration, and the Lagrangian-averaged scale-dependent model is used for the subgrid-scale (SGS) modeling.[19] The wind turbine aerodynamics are treated as body forces with the actuator-line model, where the lift and drag coefficients of each airfoil section along each blade are determined from tabulated data according to upstream wind speed and local angle of attack.[20] More details of wind turbine and turbulence simulator and its validations can be found in Xie and Archer[17] and Xie *et al.*[21]

The computational domain is a rectangular box with dimensions of $1000 \, \text{m} \times 500 \, \text{m} \times 500 \, \text{m}$ in the streamwise (x), lateral (y) and vertical (z) directions. A uniform Cartesian grid with resolution of $256 \times 128 \times 128$ is used. In the vertical direction, a wall model yielding the Monin–Obukhov similarity is used at the first grid point off the wall.[19] Note that this resolution is sufficient to capture the law of the wall near the surface and a sensitivity test of resolution of the code was performed in Xie *et al.*[21] The surface roughness height z_0 is $0.0002 \, \text{m}$, representing a calm open ocean surface, and the slip and no-penetration conditions are used at the top of the domain for the horizontal velocity components and vertical velocity component, respectively.[17] The flow is driven by a fixed streamwise geostrophic wind of $16 \, \text{m s}^{-1}$ at the top with a vertical damping layer above $450 \, \text{m}$.[22] The atmospheric boundary layer (ABL) is treated as neutral, i.e., buoyant effects are negligible. First of all, a precursor simulation is performed without wind turbines, in order to fully develop the turbulence in the ABL. The time and horizontally averaged vertical profiles of mean wind speed, total kinematic shear stress and resolved turbulence kinetic energy (TKE) of the precursor simulation are plotted in Figure 1.

Then, after the precursor simulation, two types of wind turbines are added to the ABL. The first is a large HAWT, the REpower 5 MW model, placed at $x = 500 \, \text{m}$ and $y = 250 \, \text{m}$. The hub height is $H_H = 88 \, \text{m}$, and the diameter of the rotor is $D = 126 \, \text{m}$. Besides the large HAWT, we also consider a layer of smaller wind turbines, which in this case are VAWT. The VAWT can be considered as 'H' type or 'Giromill' type,[23] with a capacity of about $50 \, \text{kW}$. The 'hub height' is $H_V = 15 \, \text{m}$ (i.e., the tower height, but the term hub height is used here in analogy to the HAWT), the blade length is $h = 20 \, \text{m}$ and the rotor diameter is $w = 10 \, \text{m}$, giving a rotor area of $A_V = hw = 200 \, \text{m}^2$. Note that the top-tip height of the VAWT is equal to the bottom tip height of the HAWT, which is a compromise between keeping the dimensions of all the wind turbines realistic and having enough resolution for the numerical simulations (i.e., sufficient grid points to cover the actuator disk of the VAWTs and at least one grid level below the rotor of VAWTs). In this study, 20 VAWTs are considered and evenly distributed around each HAWT in the wind farm (Figure 2). The HAWT is parameterized using the default actuator-line model, whereas the smaller VAWTs are modeled by the actuator-disk model[24,25] with a thrust coefficient of 0.25[26] due to relatively low grid resolution in their rotor regions. As a comparison, a traditional wind farm with only the HAWT is simulated using the same setup, and it is referred to as the control wind farm throughout the paper. Note that, because periodic boundaries are imposed in the horizontal
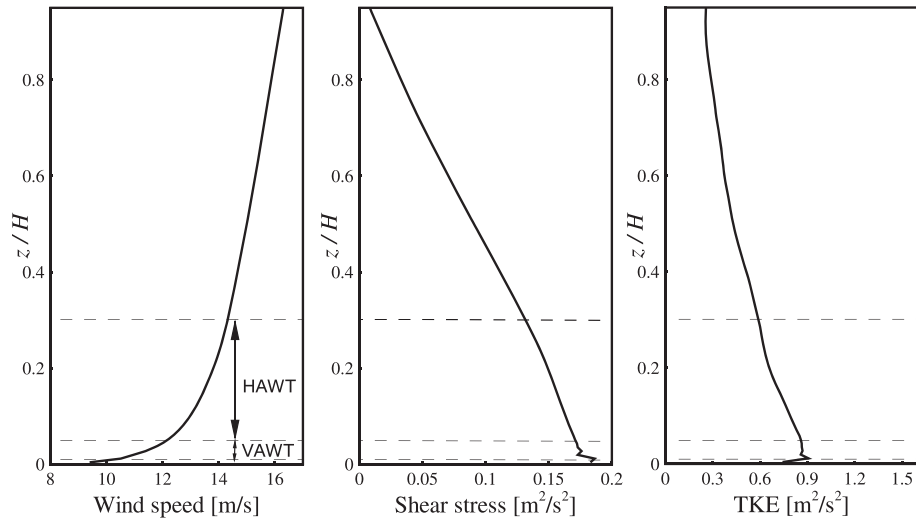
Figure 1. Vertical profiles of the atmospheric boundary layer from the precursor simulation.
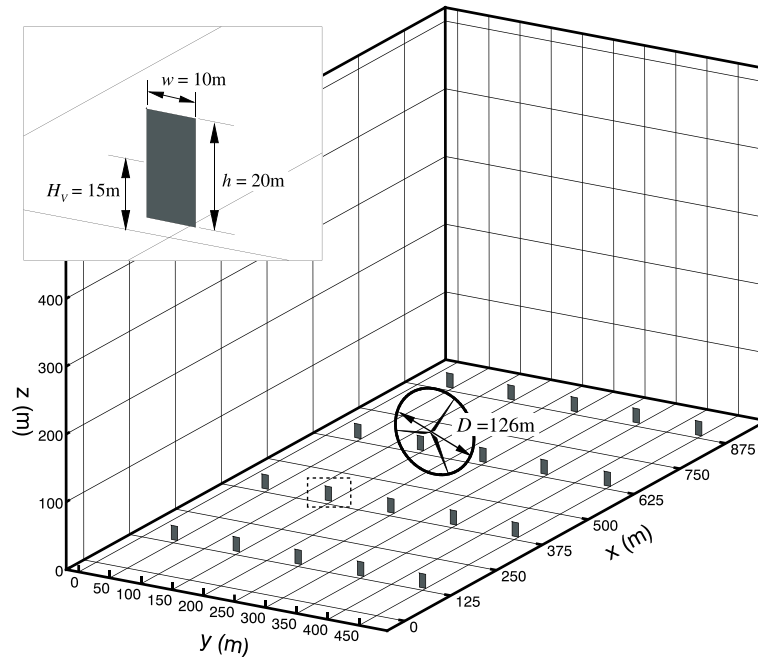

Figure 2. Layout of the infinitely large vertically staggered wind farm. The VAWTs are represented by filled rectangles. The upper-left figure is a zoomed-in view of the rectangular region surrounding a VAWT denoted by dashed lines.

directions,[22,24,25] the current setup represents effectively an infinitely large wind farm with spacing of 7.9D and 4D between each HAWT along the x and y directions.

2.2. Large-eddy simulation results

The power extracted from the wind can be estimated from following definition:

$$P = T \cdot U_d, \tag{1}$$

where T is the total thrust force exerted by the wind turbine and U_d is the resolved streamwise velocity averaged over the turbine rotor region. The thrust force T can be calculated from the actuator-line model for the HAWT or the actuator-disk

model for the VAWTs. Note that equation 1 gives an estimation of power extracted from the wind, which is not the electric power produced by the wind turbines. The extracted power is always higher than the generated power because of various losses, but the distinction is not important for the purposes of relative comparisons. Because we only simulate one periodic cell of turbines (1 HAWT plus 20 VAWTs for the VS wind farm, or 1 HAWT for the control wind farm) as a representation of the infinite wind farm, the power mentioned hereafter should be considered as 'per cell'.

As shown in Figure 3, when the power output reaches a quasi-steady state, the mean power extracted by the HAWT alone is higher (about 10%) in the VS than in the control farm, although its power fluctuations are also larger (in terms of standard deviation). When the VAWTs are added, which contribute approximately an extra 700 kW, the total power generation from the VS farm is about 4.2 MW, which is 32% higher than that from the control farm. Meanwhile, the power fluctuations are slightly increased from 12.7% to 15.4%. Nonetheless, the VS technique improves the performances, in terms of mean power production, of both the overall wind farm and the HAWT alone, while the fatigue loads may also increase. Note that our goal is to improve the performance of an existing HAWT wind farm, but not to compare the VS farm with the summation of two independent HAWT and VAWT farms. That is to say, we consider a fixed amount of available land area and inquire about maximum possible power production for that area. A more detailed economic analysis to find a real optimal wind farm strategy (as carried out in Meyers and Meneveau[27]) would introduce dependencies on the ratio of land versus HAWT and VAWT costs and falls outside of the scope of this paper.

The spectrum of the extracted power from the HAWT is obtained by performing a fast Fourier transform on the time-series data. As shown in Figure 4, a clear peak is revealed in the low-frequency range (around 0.012 Hz), corresponding to the low-frequency oscillations of upstream wakes (i.e., the wake meandering), in both the VS and control wind farms. The corresponding magnitude in the VS case is larger than in the control case, and the peak frequency is slightly higher in the VS case. On the other hand, in the high frequency range, the two wind farms have almost the same behaviors, and a peak coinciding with three times of the frequency of turbine rotation, as well as some resonant modes (i.e., six times), are also observable.

Next, the time-averaged resolved streamwise velocity (denoted by U) is plotted in Figure 5 for both the control and the VS wind farm. The most noticeable difference in the two wind farms is shown on the horizontal plane close to the ground, where the VAWTs induce pronounced wakes in the VS wind farm, indicating the wind energy extraction by the VAWTs. The distance between two adjacent VAWTs in the streamwise direction is $12.5\,h$, which gives sufficient space for the VAWT wakes to develop and for the wind speed to recover. Moreover, the expansion of the VAWT wakes appears to be very limited in the vertical direction, because of strong wind shear near the ground.[17] Past the HAWT, strong wakes are observed in both wind farms. Note that the HAWT wake is shorter in the VS farm than that in the control case (refer to the contour line of $9.5\,\mathrm{m\,s^{-1}}$ for instance), which contributes to the improved performance of the HAWT in the VS farm.

In order to further reveal the varying wake recovery rate in the two cases, profiles of time-averaged resolved streamwise velocity in the vertical central plane are plotted at several locations in Figure 6. In general, two competing effects are found. On one hand, the VS wind farm has lower streamwise velocity above and below the rotor region compared with the control wind farm, which can be explained as a result of the increased effective surface roughness (or more extracted wind momentum) by adding the VAWTs. On the other hand, in the rotor region, where the HAWT wake dominates, the wake recovery is faster in the VS wind farm than in the control. Therefore, in the downstream direction, the wind speed profiles are less sheared and less defected in the HAWT's rotor region in the VS farm than in the control farm.
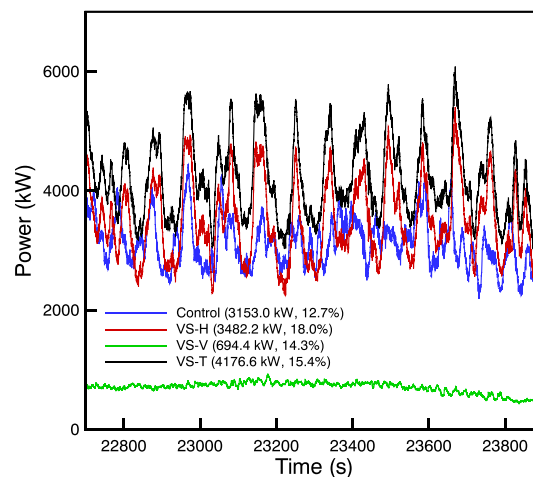

Figure 3. Power extracted from the wind by: the control farm (blue line), consisting of only HAWTs; the HAWT in the VS farm (red line); the VAWTs in the VS farm (green line); and overall VS farm (black line). The inset shows the mean value of each curve as well as its standard deviation in percentage.
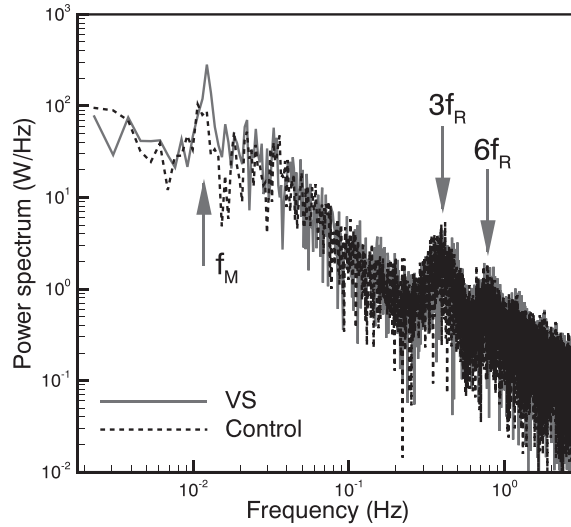
Figure 4. Spectra of power extracted from the HAWT in both VS and control wind farms. f_M and f_R denote the frequencies of wake meandering and wind turbine rotation, respectively.

In Figure 7, the distributions of Reynolds-averaged TKE (will also be referred to just as TKE in the paper for simplicity) defined as $\overline{(u_i' u_i')}/2$ are shown, where $u_i' = \tilde{u}_i - \overline{\tilde{u}}_i$ is the Reynolds velocity fluctuations and the overbar denotes the time averaging. In the HAWT wake regions, the TKE distributions are similar in the two cases, i.e., the maximum occurs directly
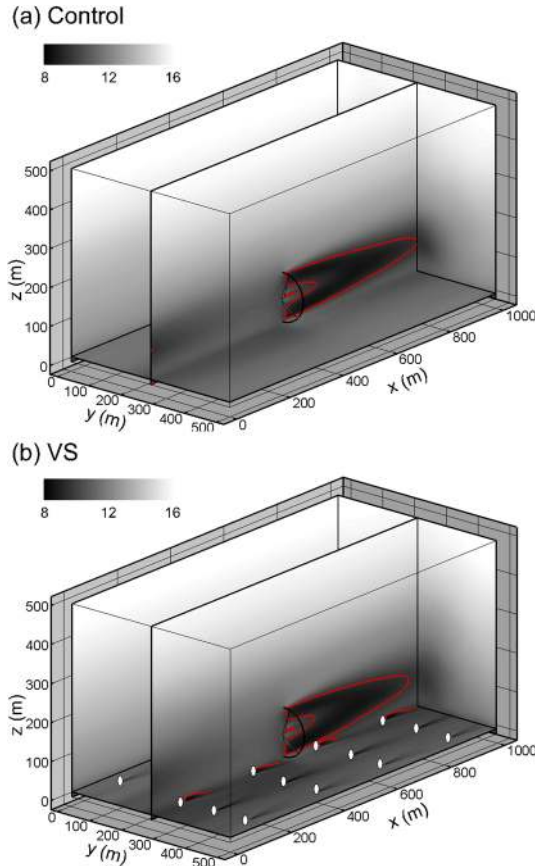

Figure 5. Distribution of time averaged resolved streamwise velocity U (m s^{-1}) at several slides in: (a) control wind farm and (b) VS wind farm. The slides are at $y = 2$ m, 250 m, $z = 15$ m and $x = 1000$ m, respectively. The red lines represent $U = 9.5$ m s^{-1}.
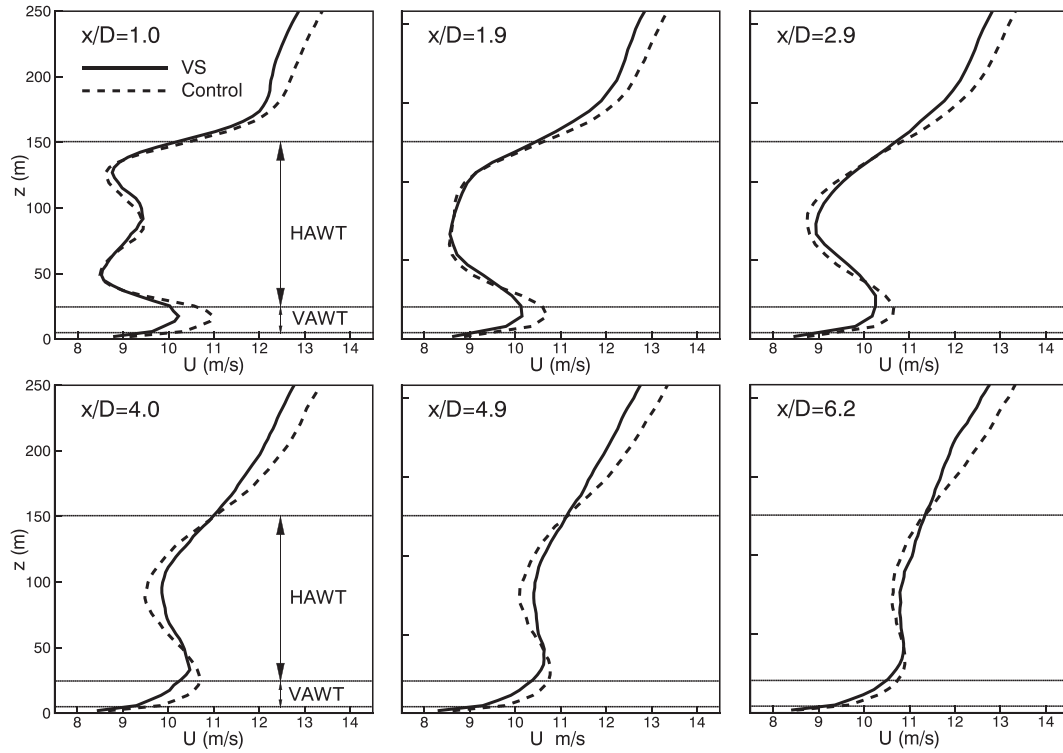
Figure 6. Vertical profiles of time averaged resolved streamwise velocity at several locations downstream of the HAWT as multiples of its diameter *D*. Note that the VAWTs are located at *x/D* = 1.0, 3.0, 5.0 and 7.0, respectively.

behind the rotor and approximately at the top-tip level where a free shear layer is formed.[17] The TKE in the HAWT wake is slightly higher in the control farm than that in the VS farm, because of larger wind shear as shown in Figure 6. However, in regions away from the HAWT wake, not only in the wakes of VAWTs but also above the VAWT layer, the TKE is discernably higher in the VS farm than that in the control farm. In other words, the TKE is more concentrated in the HAWT wake region in the control farm, but it is more evenly distributed in the VS farm. The stronger ambient turbulence enhances the mixing of the HAWT wake, which leads to faster wind speed recovery in the VS farm, as discussed earlier. An analogy can be found in the unstable ABL, where faster wake recovery was observed because of enhanced buoyancy-induced turbulence.[28] Here, unlike in the unstable ABL, the enhanced turbulence is not generated by buoyancy but because of the presence of the VAWTs.

The time and horizontally averaged (averaged in both *x* and *y* directions) Reynolds-averaged and dispersive parts of TKE, as well as their summation, are plotted in Figure 8. The dispersive part arises from the spatial inhomogeneity in the horizontal directions[24,25] and is defined as $\langle u_i'' u_i'' \rangle / 2$, where the bracket $\langle \ldots \rangle$ represents horizontal averaging and $u_i'' = \overline{\widetilde{u}_i} - \langle \overline{\widetilde{u}_i} \rangle$ are the dispersive velocity fluctuations. As expected, throughout the whole height, the VS case has larger summed TKE compared with the control case. The difference is better revealed in the Reynolds-averaged part, which is larger in the VS farm. On the other hand, the dispersive parts are comparable in the two cases except in the HAWT layer where it is larger in the control farm than in the VS farm, reflecting that the spatial inhomogeneity of TKE is stronger in the control farm.

Furthermore, the TKE rate of production (PRD) and (the negative of) the dissipation rate (DIS) are calculated using the following definitions:

$$PRD = -\overline{u_i' u_j'} \frac{\partial \overline{\overline{u}}_i}{\partial x_j}, \tag{2}$$

$$DIS = -\overline{2 v_r S_{ij}' S_{ij}'}, \tag{3}$$

where v_r is the eddy viscosity from the SGS modeling and S_{ij}' is the rate of strain tensor of the resolved velocity fluctuations. In Figure 9, profiles of horizontally averaged PRD and DIS are plotted for the two wind farms. The profiles of DIS are almost identical in the bulk region throughout the entire ABL in both wind farms, except that larger DIS is observed locally
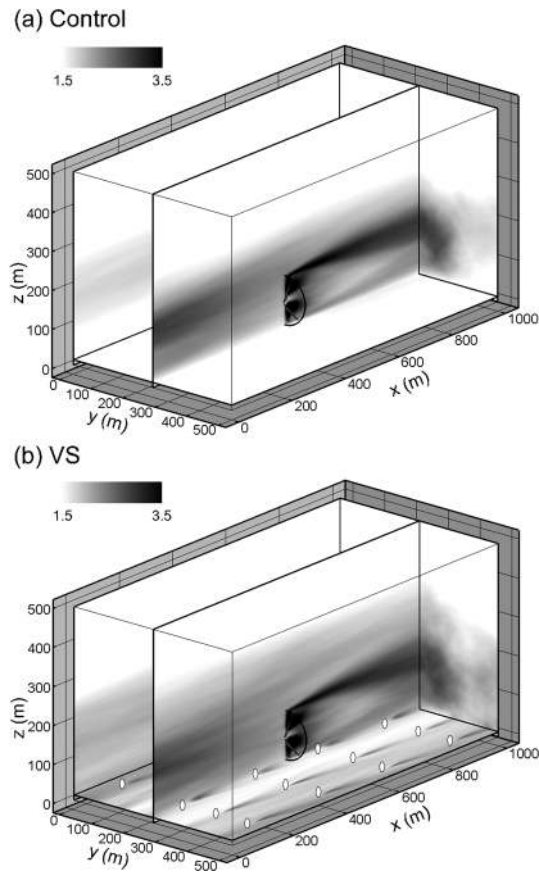
Figure 7. Distribution of Reynolds-averaged turbulent kinetic energy (m^2 s^{-2}) at several slides in (a) control wind farm, and (b) VS wind farm. The slides are at $y = 2$ m, 250m, $z = 15$ m and $x = 1000$ m, respectively.

around the VAWT layer in the VS farm. On the other hand, the influence of the VS approach on PRD is not only limited in the VAWT layer but also obvious in the HAWT layer, which results in enhanced TKE in a large extent as discussed earlier. In both of wind farms, two peaks of PRD are observed: one is around the top-tip level of the HAWT and the other is near
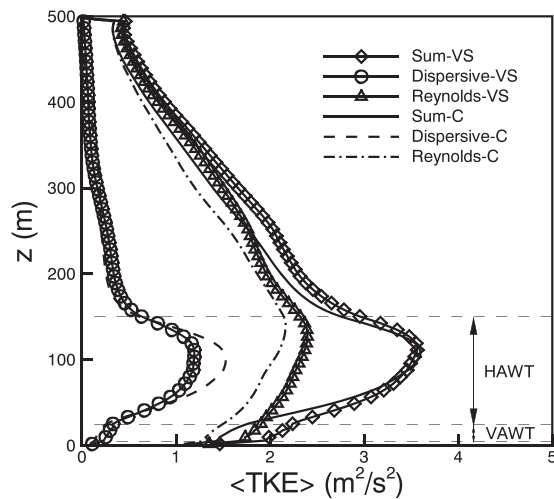

Figure 8. Vertical profiles of resolved TKE averaged in time and horizontal directions. Dotted lines: heights of top, hub and bottom levels of the HAWT, and bottom height of the VAWT. VS: vertically staggered wind farm; C: control wind farm; Sum: summation of the Reynolds-averaged and dispersive parts of the TKE.
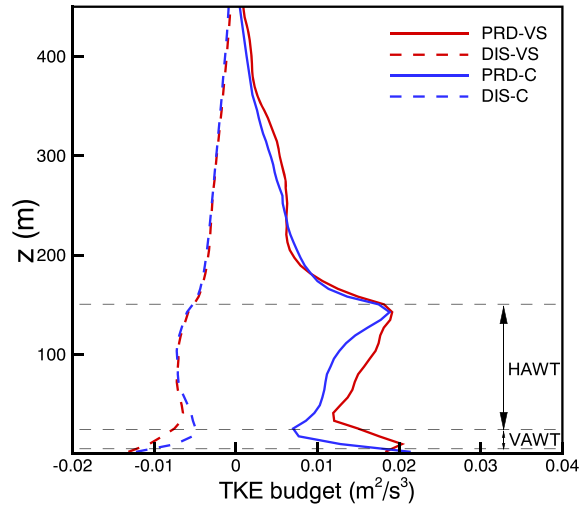
Figure 9. Vertical profiles of TKE production (PRD) and TKE dissipation rate (DIS) averaged in time and horizontal directions. VS denotes the VS farm and C the control case.

the ground. The former one is less affected by the VS approach whereas the latter one is strongly correlated to the presence of VAWTs.

Finally, the impact of vertical staggering on shear stress is analyzed. The horizontally averaged total kinematic shear stress $\langle \tau_{xz} \rangle$ can be obtained by summation of three components: the Reynolds shear stress $-\langle \overline{u'w'} \rangle$, the SGS shear stress $\langle \overline{\widetilde{uw}} - \overline{\widetilde{u}\widetilde{w}} \rangle$ (from the SGS model) and the dispersive shear stress $-\langle u''w'' \rangle$. As plotted in Figure 10, expected linear behaviors of the total shear stress are shown above the top of the HAWT canopy, and an upper friction velocity can be calculated as $u_{*,hi} = \sqrt{\langle \tau_{xz} \rangle} (z = H_H + D/2)$ (the subscript 'hi' denotes the 'high' layer above the HAWT canopy).[24,25] From the plot, we obtain that $u_{*,hi} \approx 0.81 \, \mathrm{m \, s^{-1}}$ for the VS farm and $0.76 \, \mathrm{m \, s^{-1}}$ for the control farm. The larger $u_{*,hi}$ indicates a higher forcing impact from the wind farms to the ABL.[25] In the rotor region of HAWT, linear depletions occur as a result of extraction of momentum flux. It is found that the amounts of depletion are almost the same in the two farms. Below the HAWT, the total shear stress increases towards the ground in the control case, whereas it keeps being depleted by the VAWTs in the VS case until the bottom tip the VAWTs. We find that the lower friction velocity defined as $u_{*,lo} = \sqrt{\langle \tau_{xz} \rangle} (z = 0)$ (the subscript 'lo' denotes the 'low' layer below the wind-turbine layers) is slightly smaller in the VS farm (about $0.40 \, \mathrm{m \, s^{-1}}$) than that in the control farm (about $0.42 \, \mathrm{m \, s^{-1}}$).
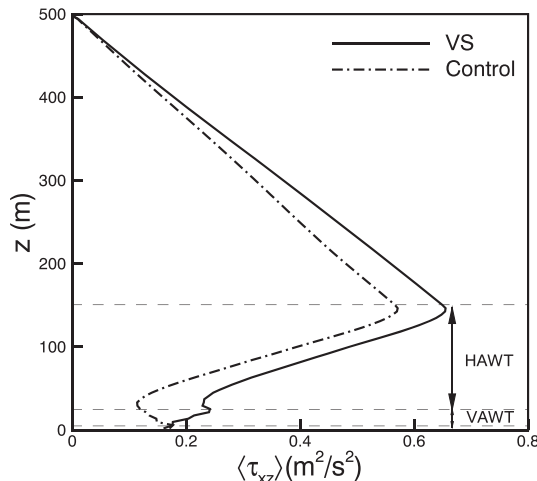

Figure 10. Vertical profiles of the total kinematic shear stress ($\mathrm{m^2 \, s^{-2}}$) averaged in time and horizontal directions for both the VS and control farms.

3. ANALYTICAL MODEL

3.1. Model description

Numerous low-order models are available to study the wind farm wakes, each focusing on different aspects of the problem.[26,29–32] Following the assumption of infinitely large, fully developed wind farm as in the previous section, an analytical 'top-down' model, primarily developed by Frandsen[33,34] and Calaf *et al.*[24] and later extended to a large but finite-size wind farms by Meneveau,[35] was modified here to take into account the vertical staggering and addition of VAWT.

In the original models for conventional wind farms, e.g., the control wind farm used in this study, three layers are assumed throughout the wind farm ABL (of height H): two log layers below and above the HAWT rotor region and a wake layer in the rotor region modeled by additional eddy viscosity. The upper and lower log regions are characterized by the upper and lower friction velocities $u_{*,hi}$ and $u_{*,lo}$, respectively. In the upper log layer, the presence of the wind farm induces the so-called wind-farm effective surface roughness height $z_{0,hi}$. Following this idea, in this work, we divide the boundary layer into five layers (Figure 11), i.e., two wake layers in the rotor regions of HAWT and VAWT, with enhanced eddy viscosities and three log layers (besides the hi and lo log layers, a middle 'mi' log layer is assumed in between the two wake layers), as follows:

1. Log layer between the ground and the bottom of the VAWTs, characterized by a surface roughness $z_{0,lo}$ and friction velocity $u_{*,lo}$ as follows:

$$u(z) = \frac{u_{*,lo}}{\kappa} \ln\left(\frac{z}{z_{0,lo}}\right), \; z_{0,lo} < z < H_V - \frac{h}{2},$$ (4)

where H_V and h are hub height and rotor height of the VAWT;

2. Wake layer covering the rotor area of the VAWTs, in which the effect of the VAWTs can be parameterized as an added, uniform and constant eddy viscosity ν_V:

$$(\kappa z u_* + \nu_V)\frac{du(z)}{dz} = u_*{}^2, \; H_V - \frac{h}{2} < z < H_V + \frac{h}{2}$$ (5)

where the eddy viscosity ν_V can be estimated as

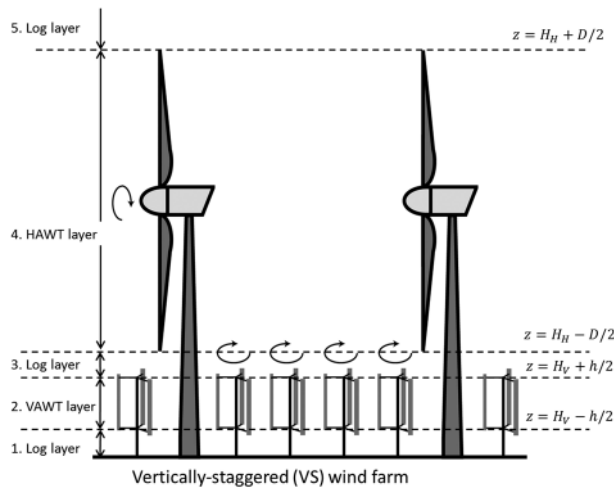$$\nu_V \approx \sqrt{\frac{c_V^{ft}}{2}} u(H_V) w,$$ (6)

Figure 11. Sketch of the five layers in the VS mixed wind turbine array boundary layer.

where $\sqrt{c_V^{ft}/2}\, u(H_V)$ is a characteristic velocity scale due to momentum defect, and w is the relevant characteristic length scale (as the integral length scale of vortices from a VAWT are of the order of the rotor diameter). Equation 5 can be rewritten as

$$\left(1 + v_V^*\right)\frac{du(z)}{d\ln\left(\frac{z}{H_V}\right)} = \frac{u_*}{\kappa},$$
(7)

where v_V^* is the effective eddy viscosity estimated as

$$v_V^* = \frac{v_V}{\kappa u_* z}.$$
(8)

Further in equation 6, c_V^{ft} is the loading coefficient of the VAWT,[24,25,35] which is a function of the thrust coefficient C_T^V, the rotor area of the VAWTs A_V and the horizontal spacing between VAWTs in the streamwise and spanwise directions S_V^x and S_V^y

$$c_V^{ft} = \frac{C_T^V A_V}{S_V^x S_V^y} = \frac{C_T^V h w}{S_V^x S_V^y}.$$
(9)

The effective added viscosity v_V^* is evaluated at H_V and is no longer a function of z,[24] and the choice of the respective friction velocity u_* will be discussed shortly;

3 Log layer between the top of the VAWTs and the lower tip of the larger HAWTs, characterized by $z_{0,mi}$ and $u_{*,mi}$:

$$u(z) = \frac{u_{*,mi}}{\kappa}\ln\left(\frac{z}{z_{0,mi}}\right), \quad H_V + \frac{h}{2} < z < H_H - \frac{D}{2},$$
(10)

where H_H and D are hub height and diameter of the HAWT;

4 Wake layer covering the rotor area of the large HAWTs, in which again the effect of the wind turbine is parameterized as an added, uniform and constant eddy viscosity v_H:

$$\left(1 + v_H^*\right)\frac{du(z)}{d\ln\left(\frac{z}{H_H}\right)} = \frac{u_*}{\kappa}, \quad H_H - \frac{D}{2} < z < H_H + \frac{D}{2},$$
(11)

where

$$v_H^* = \frac{v_H}{\kappa u_* H_H}, \text{ and } v_H \approx \sqrt{\frac{c_H^{ft}}{2}}\, u(H_H) D$$
(12)

$$c_H^{ft} = \frac{C_T^H A_H}{S_H^x S_H^y} = \frac{C_T^H \pi D^2}{4 S_H^x S_H^y};$$
(13)

5 Log layer above the HAWTs with $z_{0,hi}$ and $u_{*,hi}$

$$u(z) = \frac{u_{*,hi}}{\kappa}\ln\left(\frac{z}{z_{0,hi}}\right), \quad H_H + \frac{D}{2} < z < H.$$
(14)

Next, with the earlier assumptions, we derive analytical expressions for wind speed at the respective hub heights of the VAWTs and HAWTs. Focusing first on layer 2, equation 7 can be integrated in the vertical direction by matching the velocities at the top and bottom of the layer to those in layer 1 and 3, respectively, to obtain the following:

$$u(z) = \frac{u_{*,lo}}{\kappa} ln\left[\left(\frac{z}{H_V}\right)^{\frac{1}{1+v_{V,l}^*}}\left(\frac{H_V}{z_{0,lo}}\right)\left(\frac{H_V - \frac{h}{2}}{H_V}\right)^{\frac{v_{V,l}^*}{1+v_{V,l}^*}}\right], \quad H_V - \frac{h}{2} \le z < H_V, \tag{15}$$

$$u(z) = \frac{u_{*,mi}}{\kappa} ln\left[\left(\frac{z}{H_V}\right)^{\frac{1}{1+v_{V,u}^*}}\left(\frac{H_V}{z_{0,mi}}\right)\left(\frac{H_V + \frac{h}{2}}{H_V}\right)^{\frac{v_{V,u}^*}{1+v_{V,u}^*}}\right], \quad H_V \le z < H_V + \frac{h}{2}, \tag{16}$$

where $v_{V,l}^* = \frac{v_V}{\kappa H_V u_{*,lo}}$ and $v_{V,u}^* = \frac{v_V}{\kappa H_V u_{*,mi}}$ are used below and above the hub height of the VAWT, respectively, and v_V is given by equation 6. As a result, at hub height H_V

$$u(H_V) = \frac{u_{*,lo}}{\kappa} ln\left[\left(\frac{H_V}{z_{0,lo}}\right)\left(H_V - \frac{h}{2}\right)^{\frac{v_{V,l}^*}{1+v_{V,l}^*}}\right] = \frac{u_{*,mi}}{\kappa} ln\left[\left(\frac{H_V}{z_{0,mi}}\right)\left(H_V + \frac{h}{2}\right)^{\frac{v_{V,u}^*}{1+v_{V,u}^*}}\right]. \tag{17}$$

From the momentum balance[33,35]

$$u_{*,mi}^2 = u_{*,lo}^2 + \frac{1}{2} c_V^{ft} u(H_V)^2, \tag{18}$$

$$u_{*,hi}^2 = u_{*,mi}^2 + \frac{1}{2} c_H^{ft} u(H_H)^2, \tag{19}$$

and from equation 17, we have

$$\frac{u_{*,mi}}{u_{*,lo}} = \frac{ln\left(\frac{H_V}{z_{0,lo}}\right) + \frac{v_{V,l}^*}{1+v_{V,l}^*} ln\left(\frac{H_V - \frac{h}{2}}{H_V}\right)}{ln\left(\frac{H_V}{z_{0,mi}}\right) + \frac{v_{V,u}^*}{1+v_{V,u}^*} ln\left(\frac{H_V + \frac{h}{2}}{H_V}\right)}. \tag{20}$$

Substituting equations 17 and 20 into equation 18, an analytical expression for $z_{0,mi}$ can be obtained:

$$z_{0,mi} = H_V \left(\frac{H_V + \frac{h}{2}}{H_V}\right)^{\frac{v_{V,u}^*}{1+v_{V,u}^*}} exp\left(-\left[\frac{c_V^{ft}}{2\kappa^2} + \left\{ln\left[\frac{H_V}{z_{0,lo}}\left(\frac{H_V - \frac{h}{2}}{H_V}\right)^{\frac{v_{V,l}^*}{1+v_{V,l}^*}}\right]\right\}^{-2}\right]^{-1/2}\right). \tag{21}$$

Note that $v_{V,l}^*$ and $v_{V,u}^*$ are unknown, and they are dependent on $z_{0,mi}$, $u_{*,mi}$ and $u_{*,lo}$. A simple iteration method is used to solve them by initially setting $z_{0,mi} = z_0$ and $u_{*,lo} = u_{*,mi} = u_*$. Similarly for level 4, with the HAWT, the following relationships are obtained:

$$u(H_H) = \frac{u_{*,hi}}{\kappa} ln\left[\left(\frac{H_H}{z_{0,hi}}\right)\left(H_H + \frac{D}{2}\right)^{\frac{v_{H,u}^*}{1+v_{H,u}^*}}\right] = \frac{u_{*,mi}}{\kappa} ln\left[\left(\frac{H_H}{z_{0,mi}}\right)\left(H_H - \frac{D}{2}\right)^{\frac{v_{H,l}^*}{1+v_{H,l}^*}}\right] \tag{22}$$

$$\frac{u_{*,hi}}{u_{*,mi}} = \frac{ln\left(\frac{H_H}{z_{0,mi}}\right) + \frac{v_{H,l}^*}{1+v_{H,l}^*} ln\left(\frac{H_H - \frac{D}{2}}{H_H}\right)}{ln\left(\frac{H_H}{z_{0,hi}}\right) + \frac{v_{H,u}^*}{1+v_{H,u}^*} ln\left(\frac{H_H + \frac{D}{2}}{H_H}\right)} \tag{23}$$

$$z_{0,hi} = H_H \left(\frac{H_H + \frac{D}{2}}{H_H} \right)^{\frac{v_{H,u}^*}{1+v_{H,u}^*}} exp \left(- \left[\frac{c_H^{ft}}{2\kappa^2} + \left\{ ln \left[\frac{H_H}{z_{0,mi}} \left(\frac{H_H - \frac{D}{2}}{H_H} \right)^{\frac{v_{H,l}^*}{1+v_{H,l}^*}} \right] \right\}^{-2} \right]^{-1/2} \right) \tag{24}$$

where $v_{H,l}^* = \frac{v_H}{\kappa H_H u_{*,mi}}$ and $v_{H,u}^* = \frac{v_H}{\kappa H_H u_{*,hi}}$, and v_H is given by equation 12. Now, the only unknown is $u_{*,hi}$, which can be derived from the geostrophic relationship:

$$u_{*,hi} = \frac{\kappa U_G}{ln\left(\frac{U_G}{f z_{0,hi}}\right) - C}, \tag{25}$$

where $C \sim 4.5$ is a standard empirical value for neutral ABL,[35] U_G is the geostrophic wind speed and f is the Coriolis parameter. Here, because the Coriolis forcing is not considered, equation 25 can be simplified as follows:

$$u_{*,hi} = \frac{\kappa U_G}{ln\left(\frac{H_G}{z_{0,hi}}\right)}, \tag{26}$$

where H_G is the boundary layer height where U_G is imposed. In Appendix A, a flowchart summarizing the model is provided in Figure 15. Note that it is not necessary to have the intermediate log layer between the VAWTs and HAWTs (i.e., the third layer), when the top-tip level of the VAWTs and bottom tip level of the HAWTs are coincident (although no overlap between the two rotor regions is permitted). However, as in Section 2, $z_{0,mi}$ and $u_{*,mi}$ are still calculated as described earlier and used in the equations of the other parameters.

3.2. Analytical results of the VS wind farm

In this section, the performance of the VS wind farm is evaluated using the analytical top-down model described earlier. From the LES results in Section 2.2, the thrust coefficients of the HAWT were found to be $C_T^H \approx 0.59$ in the VS case and 0.54 in the control case. Note that the determination of the thrust coefficient is sensitive to the choice of upstream reference velocity. Here, the streamwise velocity at $D/2$ in front of the HAWT averaged over the rotor region was used. Following Stevens *et al.*,[36] an effective spacing in the lateral direction S_{eff}^y should be used instead of S^y in equations 9 and 13, in order to produce the correct wake expansion. In principle, the effective spacing has to be determined by matching the top-down model with a wake model, which is outside the scope of the current modeling effort. For the configuration in this study, we found empirically that the following values

$$S_{H,eff}^y = 2.5D \tag{27}$$

$$S_{V,eff}^y = 4.0w \tag{28}$$

provide good matches of velocity profiles, as shown in Figure 12. In addition to the LES case with $C_T^V = 0.25$ shown earlier, another LES case with the same setup but $C_T^V = 0.50$ is also included hereafter. As seem in Figure 12, below the hub height of the VAWT layer, some disagreements between the model-predicted velocity and the LES are visible, most likely because of the low number of grid points in the LES in that region, as well as the assumptions inherent in the model. Still, considering the significant simplifications involved in the analytical model, one may conclude that LES and analytical results match quite well throughout most of the relevant domain height. Note that, because of the setting of the problem with the top level of the VAWTs exactly coinciding with the bottom level of the HAWTs, there is no intermediate log layer between the VAWTs and HAWTs. To provide further evidence for the layers included in the model, in Appendix B we present an LES case in which all five layers exist, exhibiting three logarithmic (but short) layers.

Unlike LES, which is computationally intensive, the analytical model enables us to investigate a wide range of combinations of variables in an efficient way. In this study, the parameters associated with the HAWTs are fixed, and only the effects of the VAWTs are of interest, e.g., by varying c_V^{ft} from 0 to 0.05 (Figure 13). Here, the height and rotor area of the VAWT are fixed, so the change of c_V^{ft} is primarily achieved by either increasing the thrust coefficient C_T^V or reducing the horizontal spacing S_V^x or S_V^y. Note that $c_V^{ft} = 0$ is equivalent to the control wind farm, and it is 0.0057 and 0.0114 in
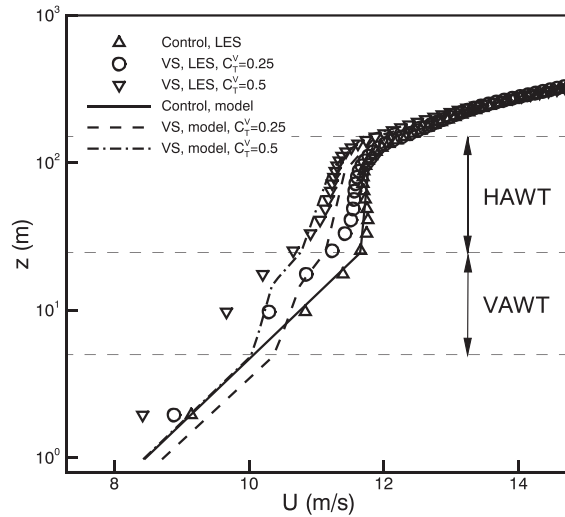
Figure 12. Comparisons of vertical profiles of time-averaged and horizontally averaged streamwise velocity from results of LES and the analytical model.

the LES with $C_T^V = 0.25$ and $C_T^V = 0.50$, respectively. While only two LES cases are presented in this paper, we find that the LES results agree well with the analytical model.

With the increase of c_V^{ft}, the velocities at the hub heights of both the HAWTs and VAWTs are decreased, as a result of increased effective surface roughness (Figure 13(a)). The reduction of available wind speed is not linear but becomes slower with the increase of c_V^{ft}. Moreover, the velocity reduction is stronger in the VAWT layer than in the HAWT layer, indicating that the wind speed at lower levels is more strongly affected by increasing the loading of VAWTs. The reduction in hub-height wind speed was also found in the LES results. However, the second effect of the VAWTs on the HAWTs from LES, namely the faster wake recovery due to stronger turbulence, is not considered in the analytical model, and therefore, the benefits of the VS wind farm will be underestimated if the analytical model is used. Despite this limitation, the analytical model is still valuable to assess the sensitivity of the VS farm to various properties of the VAWTs, as performed next.

Because no thrust force can be obtained directly from the analytical model, the wind power from the VAWTs and the HAWT can be estimated as follows:

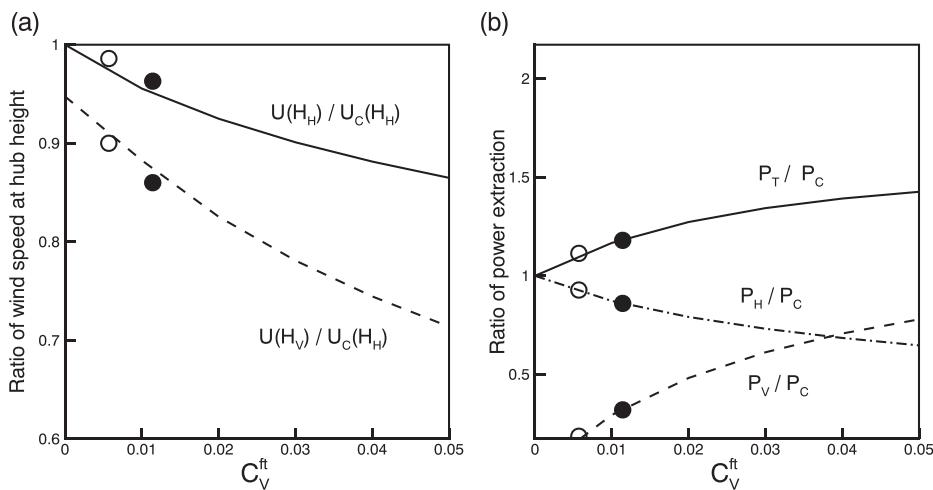**Figure 13.** Ratios of (a) wind speeds at the hub heights and (b) plane-averaged unit power extraction from the analytical model as a function of c_V^{ft}. The lines are model predictions, the open circles are LES results with $C_T^V = 0.25$ and the filled circles are LES results with $C_T^V = 0.50$. The subscript 'C' denotes the control wind farm, 'V' for 'VAWT', 'H' for 'HAWT' and 'T' for 'total'.
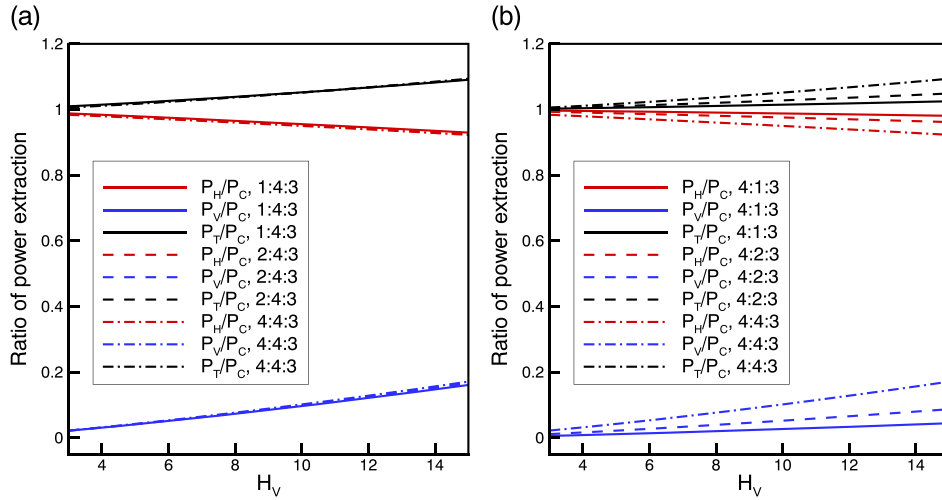
Figure 14. Ratios of the plane-averaged unit power of the VS farm as a function of hub height of VAWTs from the analytical model. The aspect ratio of VAWTs, $w : h : H_V$, is shown for each case in the legend. In (a), the ratio $h : H_V$ is fixed, and in (b) the ratio $w : H_V$ is fixed. The subscript 'C' denotes the control wind farm, 'V' for 'VAWT', 'H' for 'HAWT' and 'T' for 'total'.

$$P_V = \frac{1}{2}\rho_a c_V^{ft}\langle\overline{u}(H_V)\rangle^3, \tag{29}$$

$$P_H = \frac{1}{2}\rho_a c_H^{ft}\langle\overline{u}(H_H)\rangle^3, \tag{30}$$

where ρ_a is the air density. The power calculated here is not the same as the power shown in Figure 3, because this is actually power per horizontal unit area around the turbine clear of turbines of the same type (note that $S_H^x S_{H,eff}^y$ and $S_H^x S_{H,eff}^y$ are in the denominator of the definition of c_H^{ft} and c_V^{ft}, respectively), and the plane-averaged velocity at hub height $\langle\overline{u}(H_H)\rangle$ or $\langle\overline{u}(H_V)\rangle$ is used instead of U_d. Thus, we use the term 'plane-averaged unit power' (or just unit power for simplicity) here to distinguish among these concepts. We found that the slight decrease in P_H with c_V^{ft} is more than compensated for by P_V (Figure 13(b)), and therefore, the total $P_T = P_H + P_V$ increases with c_V^{ft} in the range considered here. Consistent with the velocity variations at the hub heights, the changes in the total unit power become more gentle with larger c_V^{ft}. Intuitively, the increase of VAWT loading may not always be beneficial to the overall farm performance, because the aloft wind speed could be reduced to the point that the energy loss by the large turbines may not be compensated by the gain from VAWTs. A maximum power ratio of 1.5 in the VS wind farm is found at $c_V^{ft} \approx 0.12$, but it is not shown here because of lack of LES data for validation.

The impact of the dimensions of VAWTs on the performance of the VS farm is investigated using the analytical model. In Figure 14, the power extraction in the VS farm relative to that in the control farm is plotted as a function of hub height H_V ranging from 3 to 15 m (the rotor area varies accordingly). The thrust coefficient $C_T^V = 0.25$ is used here. The unit power from HAWTs decreases with H_V, but the unit power from VAWTs increases even faster. Therefore, the total unit power increases almost linearly with H_V. The aspect ratios of the VAWTs, defined as $w : h : H_V$ (i.e., rotor diameter: blade height: hub height), also have an impact. As shown in Figure 14(a), when the ratio $h : H_V$ is fixed, the infinitely large VS farm is almost insensitive to the change of rotor diameter. On the other hand, the performance is clearly more influenced by the blade length, as shown in Figure 14(b), and the unit power increases with $h : H_V$.

4. DISCUSSION AND CONCLUSIONS

In this paper, we consider vertical staggering as a method to improve the energy production in large wind farms. Two types of wind turbines are considered in a wind farm, i.e., large, horizontal-axis turbines and small, vertical-axis turbines, which form two layers staggered in the vertical direction. We use both numerical and analytical methods to study this VS wind farm.

For the LES, periodic boundary conditions are used in all horizontal directions to mimic an infinite wind farm, an idealized condition in which transport and variability from flow scales larger than the domain size are neglected. The VS farm is compared with a conventional layout with only HAWTs (control farm). We find that the VS farm, with 20 VAWTs around each HAWT, can extract about 32% more power from the wind than the control wind farm and that the power extracted by the HAWT alone is also increased by about 10%. Because of the presence of the VAWT layer, the turbulence in the wind farm is increased, which enhances the wake recovery of the HAWT. The faster wake recovery more than compensates for the additional momentum loss in the wind because of increased effective surface roughness associated with the VAWTs.

A theoretical top-down model is developed for the infinite, fully developed, VS wind farm, in which five distinct layers (three log layers and two wake layers) are assumed to form throughout the boundary layer. The results show that the total momentum loss increases with either an increase of the thrust coefficient or a decrease of the spacing between VAWTs, the ratio of which is called the loading coefficient. Moreover, the analytical model shows that the total power increases with the loading coefficient in the range close to the LES configurations, but a maximum power may be reached at some high loading values. The sensitivity of the dimensions of VAWTs is studied by the analytical model as well, which indicates that, when the thrust coefficient is fixed, the total power increases almost linearly with the height of VAWTs while it is not sensitive to the width of the rotor.
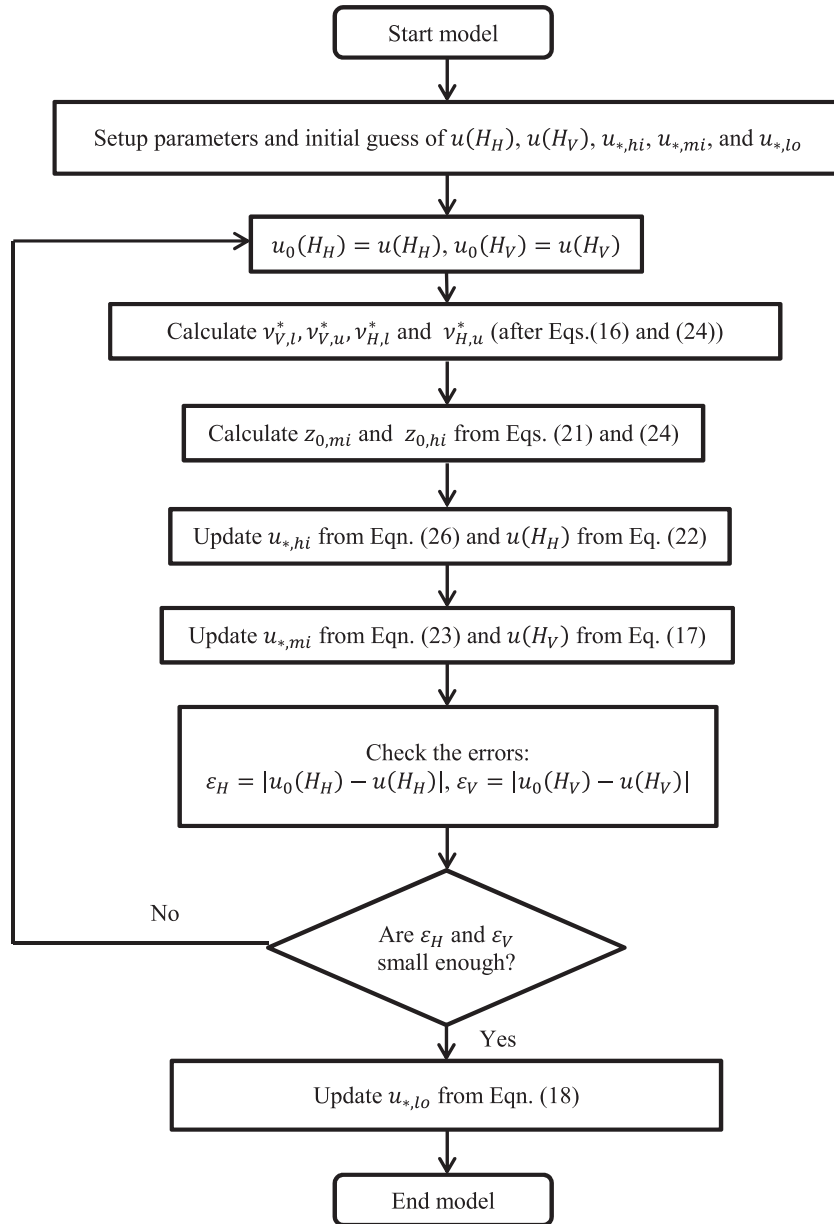
Furthermore, it is helpful to compare the VS approach with the conventional approach of adding more HAWTs. By adding another 5 MW HAWT in the x direction in the same domain, the distance between two HAWTs is reduced by half, e.g., from 8D to 4D, which leads to a wake loss of about 33% (averaged over all wind directions, such as showed for the Lillgrund wind farm[37]) for each turbine. Therefore, the total power of two HAWTs is roughly 6.7 MW, which is higher than the current LES result of the VS farm (4.2 MW). However, the capital cost of a 5 MW turbine is roughly \$10m, while twenty 50 kW VAWTs cost about \$5m.[38] Therefore, the VS approach has a better capital cost per MW than the conventional one (1.19 vs. 1.49). Therefore, adding more HAWTs may be less beneficial than adding VAWT although the economically optimal arrangement depends upon capital and operating costs as well as the price of energy and land costs.

Despite the great potential shown in this study, there are still numerous issues that are not addressed here but will be included in our future research. It is more realistic from the application point of view to study finite-size wind farms with both LES and the analytical model. The atmospheric stability should be considered, which strongly influences the turbulence in the ABL and hence wake properties.[28] Moreover, the VAWT wakes should be simulated using more sophisticated models, e.g., the actuator-line model, which leads to a better understanding of the wake interactions and possibly to the optimization of the VAWT placement. It is also important to assess the sensitivity of the VS wind farm to changes in wind direction. Even though it is known that even slight misalignments between the orientation of the rows and columns of turbines and the wind direction can lead to large differences in wake losses and therefore power output, it is expected that adding VAWTs will still be beneficial at the end, after considering all wind directions. The effect of wind direction on VS farms is likely to be different from the effect on traditional wind farms composed of only HAWTs and needs to be studied in future. In addition, considering the small size and low height of the VAWTs, their performance may be influenced by the wake effects from the tower of the HAWT, which is not considered in this study. Last but not least, as mentioned earlier, an economic analysis is needed to evaluate the actual revenue that can be generated annually or over the lifetime of the wind farm by using vertical staggering.

ACKNOWLEDGEMENT

APPENDIX A Flowchart of the analytical model

```
┌─────────────────┐
│   Start model   │
└─────────────────┘
         │
         ▼
┌─────────────────────────────────────────────────────────────────┐
│ Setup parameters and initial guess of u(H_H), u(H_V), u_*,hi,     │
│ u_*,mi, and u_*,lo                                                │
└─────────────────────────────────────────────────────────────────┘
         │
         ▼
┌─────────────────────────────────────────┐
│ u_0(H_H) = u(H_H), u_0(H_V) = u(H_V)     │
└─────────────────────────────────────────┘
         │
         ▼
┌──────────────────────────────────────────────────────────┐
│ Calculate v*_V,l, v*_V,u, v*_H,l and v*_H,u (after Eqs.(16) and (24)) │
└──────────────────────────────────────────────────────────┘
         │
         ▼
┌──────────────────────────────────────────────────┐
│ Calculate z_0,mi and z_0,hi from Eqs. (21) and (24) │
└──────────────────────────────────────────────────┘
         │
         ▼
┌──────────────────────────────────────────────────────────┐
│ Update u_*,hi from Eqn. (26) and u(H_H) from Eq. (22)       │
└──────────────────────────────────────────────────────────┘
         │
         ▼
┌──────────────────────────────────────────────────────────┐
│ Update u_*,mi from Eqn. (23) and u(H_V) from Eq. (17)       │
└──────────────────────────────────────────────────────────┘
         │
         ▼
┌──────────────────────────────────────────────────────────┐
│ Check the errors:                                          │
│ ε_H = |u_0(H_H) − u(H_H)|, ε_V = |u_0(H_V) − u(H_V)|        │
└──────────────────────────────────────────────────────────┘
         │
         ▼
     ◇ Are ε_H and ε_V small enough? ◇ ──No──→ (loop back)
         │ Yes
         ▼
┌──────────────────────────────────────────┐
│ Update u_*,lo from Eqn. (18)              │
└──────────────────────────────────────────┘
         │
         ▼
┌─────────────────┐
│   End model     │
└─────────────────┘
```

Start model

Setup parameters and initial guess of $u(H_H)$, $u(H_V)$, $u_{*,hi}$, $u_{*,mi}$, and $u_{*,lo}$

$u_0(H_H) = u(H_H)$, $u_0(H_V) = u(H_V)$

Calculate $v^*_{V,l}$, $v^*_{V,u}$, $v^*_{H,l}$ and $v^*_{H,u}$ (after Eqs.(16) and (24))

Calculate $z_{0,mi}$ and $z_{0,hi}$ from Eqs. (21) and (24)

Update $u_{*,hi}$ from Eqn. (26) and $u(H_H)$ from Eq. (22)

Update $u_{*,mi}$ from Eqn. (23) and $u(H_V)$ from Eq. (17)

Check the errors:
$\varepsilon_H = |u_0(H_H) - u(H_H)|$, $\varepsilon_V = |u_0(H_V) - u(H_V)|$

Are ε_H and ε_V small enough?

No

Yes

Update $u_{*,lo}$ from Eqn. (18)

End model

APPENDIX B Simulations of a case with five distinct layers

In the main text, we have set up the HAWT following the realistic dimensions of the offshore REpower 5 MW turbine (i. e., the hub height is 87.6 m). For the small VAWTs, the rotor area must be covered by sufficient grid points for the modeling accuracy. Considering the resolution we used (about 4 m in each direction), we had to make the rotor area of VAWT as large as possible (200 m^2 here) and its tower as high as possible (15 m^2 here) to give at least one level of grid below the rotor of VAWTs. As a result, in the LES there was no middle log layer between the HAWT and VAWT.

In order to provide further evidence from LES for the five layer assumption used in the top-down model, we add a new test case here: the parameters of the ABL and the rotor of the HAWT are identical to those used in Section 2.2, except that the hub height is increased from 88 to 110 m, while VAWTs with $H_V = 15$ m, $h = 15$ m and $w = 12$ m are considered here. Therefore, a gap of 24.5 m exists between the top-tip level of the VAWTs and bottom tip level of the HAWTs. The domain height of 600 m with finer resolution of 2 m is used here, whereas the horizontal domain size and resolution remain as in Section 2.2.
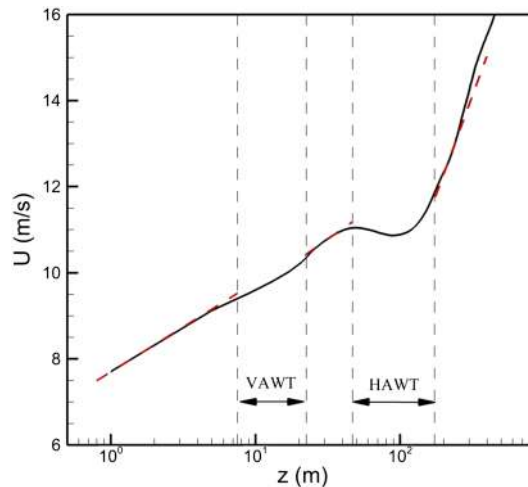
Figure 15. Vertical profile of time-averaged and horizontally averaged streamwise velocity from the LES results, showing the five layer property used in the analytical top-down model. The red dashed lines denote the three log layers.

As shown in Figure 15, the three logarithmic layers, i.e., below the VAWTs, above the HAWTs, and in between of VAWTs and HAWTs, can be discerned, whereas larger velocity deficits are observed in the two layers of wind turbines. The LES results show a clear separation of the various layers explicitly, as validation of the assumptions used in the analytical model in Section 3.1. However, because of the larger computational costs and less realistic dimensions of the turbines associated with this simulation, we do not use this particular case for the main body of our analysis and conclusions.

REFERENCES

1. Crespo A, Hernandez J, Frandsen S. Survey of modelling methods for wind turbine wakes and wind farms. *Wind Energy* 1999; **2**: 1–24.
2. Barthelmie RJ, Rathmann O, Frandsen ST, Hansen KS, Politis E, Prospathopoulos J, Rados K, Cabezón D, Schlez W, Phillips J, Neubert A, Schepers JG, van der Pijl SP. Modelling and measurements of wakes in large wind farms. *Journal of Physics: Conference Series* 2007; **75**: 012049.
3. Barthelmie RJ, Pryor SC, Frandsen ST, Hansen KS, Schepers JG, Rados K, Schlez W, Neubert A, Jensen LE, Neckelmann S. Quantifying the impact of wind turbine wakes on power output at offshore wind farms. *Journal of Atmospheric and Oceanic Technology* 2010; **27**: 1302–1317.
4. Corten GP, Schaak P, Hegberg T. Turbine interaction in large offshore wind farms. ECN Report 2004; ECN-C-04-048.
5. Archer CL, Colle BA, Monache LD, Dvorak MJ, Lundquist J, Bailey BH, Beaucage P, Churchfield MJ, Fitch AC, Kosovic B, Lee S, Moriarty PJ, Simao H, Stevens RJAM, Veron D, Zack J. Meteorology for coastal/offshore wind energy in the United States: recommendations and research needs for the next 10 years. *Bulletin of the American Meteorological Society* 2014; **95**: 515–519.
6. Stevens RJAM, Gayme D, Meneveau C. Large Eddy Simulation studies of the effects of alignment and wind farm length. *Journal of Renewable and Sustainable Energy* 2014; **6**: 023105.
7. Porté-Agel F, Wu YT, Chen CH. A numerical study of the effects of wind direction on turbine wakes and power losses in a large wind farm. *Energies* 2013; **6**: 5297–5313.
8. Chamorro LP, Arndt REA, Sotiropoulos F. Turbulent flow properties around a staggered wind farm. *Boundary-Layer Meteorology* 2011; **141**: 349–367.
9. Markfort CD, Zhang W, Porté-Agel F. Turbulent flow and scalar transport through and over aligned and staggered wind farms. *Journal of Turbulence* 2012; **13**: 1–36.
10. Wu YT, Porté-Agel F. Simulation of turbulent flow inside and above wind farms: Model validation and layout effects. *Boundary-Layer Meteorology* 2013; **146**: 181–205.
11. Archer CL, Mirzaeisefat S, Lee S. Quantifying the sensitivity of wind farm performance to array layout options using Large-Eddy Simulation. *Geophysical Research Letters* 2013; **40**: 4963–4970.
12. Chamorro LP, Tobin N, Arndt REA, Sotiropoulos F. Variable-sized wind turbines are a possibility for wind farm optimization. *Wind Energy* 2014; **17**: 1483–1494.

13. Vested MH, Hamilton N, Sørensen JN, Cal RB. Wake interaction and power production of variable height model wind farms. *Journal of Physics: Conference Series* 2014; **524**: 012169.

14. Dabiri JO, Greer JR, Koseff JR, Moin P, Peng J. A new approach to wind energy: opportunities and challenges. *AIP Conference Proceedings* 2015; **1652**: 51–57.

15. Kinzel M, Mulligan Q, Dabiri J. Energy exchange in an array of vertical-axis wind turbines. *Journal of Turbulence* 2012; **13**: 1–13.

16. Pope SB. Turbulent Flows. Cambridge University Press: New York, 2000; 558.

17. Xie S, Archer CL. Self-similarity and turbulence characteristics of wind turbine wakes via large-eddy simulation. *Wind Energy* 2015; **18**: 1815–1838.

18. Orszag SA. On the elimination of aliasing in finite-difference schemes by filtering high-wavenumber components. *Journal of Atmospheric Science* 1971; **28**: 1074–1074.

19. Bou-Zeid E, Parlange MB, Meneveau C. A scale-dependent Lagrangian dynamic model for large eddy simulation of complex turbulent flows. *Physics of Fluids* 2005; **17**: 025105.

20. Sørensen JN, Shen WZ. Numerical modeling of wind turbine wakes. *Journal of Fluids Engineering* 2002; **124**: 393–399.

21. Xie S, Ghaisas N, Archer CL. Sensitivity issues in finite-difference large-eddy simulations of the atmospheric boundary layer. *Boundary-Layer Meteorology* 2015; **157**: 421–445.

22. Lu H, Porté-Agel F. Large-eddy simulation of a very large wind farm in a stable atmospheric boundary layer. *Physics of Fluids* 2011; **23**: 065101.

23. Sutherland HJ, Berg DE, Thomas D. Ashwill TD. A retrospective of VAWT technology. *Sandia Report*; SAND2012-0304, January 2012.

24. Calaf M, Meneveau C, Meyers J. Large eddy simulation study of fully developed wind-turbine array boundary layers. *Physics of Fluids* 2010; **22**: 015110.

25. Calaf M, Parlange MB, Meneveau C. Large eddy simulation study of scalar transport in fully developed wind turbine array boundary layers. *Physics of Fluids* 2011; **23**: 126603.

26. Araya DB, Craig AE, Kinzel M, Dabiri JO. Low-order modeling of wind farm aerodynamics using leaky Rankine bodies. *Journal of Renewable and Sustainable Energy* 2014; **6**: 063118.

27. Meyers J, Meneveau C. Optimal turbine spacing in fully developed wind farm boundary layers. *Wind Energy* 2012; **15**: 305–317.

28. Abkar M, Porté-Agel F. Influence of atmospheric stability on wind-turbine wakes: a large-eddy simulation study. *Physics of Fluids* 2015; **27**: 035104.

29. Abkar M, Porté-Agel F. A new wind-farm parameterization for large-scale atmospheric models. *Journal of Renewable and Sustainable Energy* 2015; **7**: 013121.

30. Fitch AC, Olson JB, Lundquist JK, Dudhia J, Gupta AK, Michalakes J, Barstad I. Local and mesoscale impacts of wind farms as parameterized in a mesoscale NWP model. *Monthly Weather Review* 2012; **140**: 3017.

31. Yang X, Sotiropoulos F. Analytical model for predicting the performance of arbitrary size and layout wind farms. *Wind Energy* 2015. DOI: 10.1002/we.1894.

32. Ghaisas N, Archer CL. Geometry-based models for studying the effects of wind farm layout. *Journal of Atmospheric and Oceanic Technology* 2015. DOI: 10.1175/JTECH-D-14-00199.1.

33. Frandsen S. On the wind speed reduction in the center of large clusters of wind turbines. *Journal of Wind Engineering and Industrial Aerodynamics* 1992; **39**: 251–265.

34. Frandsen S, Barthelmie R, Pryor S, Rathmann O, Larsen S, Hojstrup J, Thogersen M. Analytical modelling of wind speed deficit in large offshore wind farms. *Wind Energy* 2006; **9**: 39–53.

35. Meneveau C. The top-down model of wind farm boundary layers and its applications. *Journal of Turbulence* 2012; **13**: 1–12.

36. Stevens RJAM, Gayme D, Meneveau C. Coupled wake boundary layer model of wind-farms. *Journal of Renewable and Sustainable Energy* 2015; **7**: 023155.

37. Dahlberg J-Å. Assessment of the Lillgrund windfarm: power performance wake effects. Vattenfall Vindkraft AB, 6_1 LG Pilot Report, Sept. 2009. URL: https://corporate.vattenfall.se/globalassets/sverige/om-vattenfall/om-oss/var-verksamhet/vindkraft/lillgrund/assessment.pdf

38. Windustry. How much do wind turbines cost? URL: http://www.windustry.org/how_much_do_wind_turbines_cost